The Cryosphere Discuss., doi:10.5194/tc-2016-73, 2016
Manuscript under review for journal The Cryosphere
Published: 18 April 2016

The Cryosphere Discussions
Open Access
EGU

Distributed snow and rock temperature modelling in steep rock walls using Alpine3D

Anna Haberkorn[1,2], Nander Wever[1,3], Martin Hoelzle[2], Marcia Phillips[1], Robert Kenner[1], Mathias Bavay[1], Michael Lehning[1,3]

[1]WSL Institute for Snow and Avalanche Research SLF, CH-7260 Davos, Switzerland
[2]Department of Geosciences, Unit of Geography, University of Fribourg, CH-1700 Fribourg, Switzerland
[3]CRYOS, School of Architecture, Civil and Environmental Engineering, EPFL, CH-1015 Lausanne, Switzerland
Correspondence to: Anna Haberkorn (haberkorn@slf.ch)

Abstract. In this study we modelled the influence of the spatially and temporally heterogeneous snow cover on the surface energy balance and its impact on rock temperatures in two rugged, steep rock walls on the Gemsstock ridge, central Swiss Alps. The model used is the distributed, process based energy balance model Alpine3D in combination with a precipitation scaling method to introduce varying snow distribution. Near-surface rock temperatures are modelled for snow-covered and snow-free scenarios. The performance of Alpine3D, its limitations and uncertainties are discussed and evaluated against a dense network of 30 near-surface rock temperature measurements (0.1 m depth) distributed over both rock walls and high resolution (0.2 m) snow depth data derived from four winter terrestrial laser scans.

Snow cover distribution and near-surface rock temperatures are convincingly modelled in the heterogeneous rock walls. The correction of winter precipitation input using a precipitation scaling method based on terrestrial laser scans greatly improves the results. In addition, the fine-scale resolution of the model domain (0.2 m) and of the validation data allows to consider the thermal effects of the strongly varying micro-topography and micro-climate in the rock walls. Mean annual near-surface rock temperature increase by 2 °C in the shaded rock wall and of 1 °C in the sun-exposed one were measured and modelled due to the accumulation of snow. Errors in rock temperature simulations can be explained by a lack of modelled lateral heat fluxes, as well as by errors caused by interpolation of wind and shortwave radiation.

Keywords: Alpine3D, distributed energy balance modelling, impact of snow on rock temperatures, steep rock walls

1. Introduction

In the European Alps, numerous rock avalanches in large permafrost rock faces were observed during the last decades (Gruber et al., 2004b; Ravanel and Deline, 2011; Ravanel et al., 2010). The effects of climate change and permafrost degradation on rock slope stability in high Alpine regions (Davies et al., 2001; Fischer et al., 2006; Krautblatter et al., 2013; Gruber et al., 2004a) affect the safety of local communities in the densely populated Alps. Modelling the spatial permafrost distribution is therefore of great importance and has been carried out for the European Alps using regionally calibrated empirical-statistical (e.g. Hoelzle, 1996; Imhof, 1996; Gruber and Hoelzle, 2001), statistical (Boeckli et al., 2012a,b; Keller et al., 1998; Gruber, 2012) and numerical based (Fiddes et al., 2015) approaches at different spatial scales, varying from tens of meters to kilometres.

Traditional two-dimensional (2d) permafrost maps, based on statistical models, can serve as indicators of potential permafrost occurrence, but are limited in their ability to represent physical processes such as snow

The Cryosphere Discuss., doi:10.5194/tc-2016-73, 2016
Manuscript under review for journal The Cryosphere
Published: 18 April 2016

redistribution by avalanching and wind (Hoelzle et al., 2001), three-dimensional (3d) topographical effects in the ground (Noetzli et al., 2007) and transient changes (Harris et al., 2009). To capture the strong spatial variability of atmosphere-surface interactions and their modulating factors (e.g. local terrain shading, snow) that influence subsurface properties in complex topography, high-resolution physics based simulations of land surface processes are needed. Fiddes et al. (2015) used the physics based land surface model GEOtop (Endrizzi et al., 2014) to successfully model both snow cover and ground temperature evolution over the entire European Alps with a resolution of 30 m. However, this approach cannot capture the small-scale variability of the local surface energy balance and consequently of the ground thermal regime in complex, moderately inclined terrain (Gubler et al., 2011; Riseborough et al., 2008), as well as in steep rock faces with complex micro-topography (Haberkorn et al., 2015a; Hasler et al., 2011). The coarse grid resolution cannot account for phenomena such as lateral heat fluxes at the rock surface, which are defined here as heat fluxes with differing directions (parallel, vertical, as well as perpendicular to the rock surface) caused by pronounced temperature gradients induced by rock outcrops, by adjacent snow-covered and snow-free rock portions or by water flow at the rock surface. Lateral heat fluxes cause strongly variable ground surface temperatures in rock slopes (Haberkorn et al., 2015a), as well as between mountain sites (Gruber et al., 2004c; Wegmann et al., 1998) leading to substantial 3d thermal effects at depth of steep rock walls with convex topography (Noetzli et al., 2007; Noetzli and Gruber, 2009).

However, before a suitable investigation of 3d subsurface heat flow is feasible in steep bedrock, the strongly variable spatial and temporal ground surface boundary conditions and their driving factors need to be modelled realistically and with a high spatial resolution. One of these driving factors is the snow cover and its influence on the rock thermal regime, which has only recently been studied in steep bedrock (Gruber et al., 2004b; Gruber and Haeberli, 2007; Hasler et al., 2011). In steep rock walls exceeding 50° snow was often neglected for modelling purposes (Fiddes et al., 2015; Gruber et al., 2004a; Mittaz et al., 2002; Noetzli et al., 2007). In general it was assumed that wind and gravitational transport (avalanching or sloughing) remove the snow from steep rock (Blöschl and Kirnbauer, 1992; Gruber Schmid and Sardemann, 2003; Pogliotti, 2011; Winstral et al., 2002). We argue that rock temperature modelling cannot be done realistically without taking snow into account, since rock slopes in the Alps are generally heterogeneous, fractured and thus partly snow-covered (Gruber et al., 2004a; Hasler et al., 2011).

Recent studies based on terrestrial laser scanning (TLS) have shown that snow accumulates in steep, rough rock walls (Haberkorn et al., 2015a; Sommer et al., 2015; Wirz et al., 2011), especially due to micro-topographic effects, such as short distances to rock ledges on which snow can accumulate (Haberkorn et al., 2015a). The highly variable spatial and temporal distribution of the snow cover strongly influences the ground thermal regime of steep rock faces (Haberkorn et al., 2015a, b; Magnin et al., 2015) due to high surface albedo and low thermal conductivity of the snow cover, as well as energy consumption during snow melt (Bernhard et al. 1998; Keller and Gubler, 1993; Zhang, 2005). In gently inclined, blocky terrain effective ground surface insulation from cold atmospheric conditions were observed and modelled for snow depths exceeding 0.6 to 0.8 m (Hanson and Hoelzle, 2004; Keller and Gubler, 1993; Luetschg et al., 2008), while cooling effects on rock temperatures were found for snow depths smaller 0.15 m (Keller and Gubler, 1993). In contrast, Haberkorn et al. (2015a) found that snow depths exceeding 0.2 m were enough to have an insulating effect in steep, bare bedrock. Such amounts are likely to accumulate in steep, high rock walls with a certain degree of fracturing. Indeed, a warming effect of the snow cover on mean annual ground surface temperature (MAGST) was observed by Haberkorn et al. (2015a) and Magnin et al. (2015) in shaded rock walls, whilst in moderately inclined (45°-70°) sun-exposed

The Cryosphere Discuss., doi:10.5194/tc-2016-73, 2016
Manuscript under review for journal The Cryosphere
Published: 18 April 2016

rock walls Hasler et al. (2011) suggest a reduction of MAGST of up to 3 °C compared to estimates in near-vertical, compact rock, due to snow persistence during the months with most intense radiation. However, a thick snow cover smoothes the variability of MAGST between N-S oriented ridges by around 4 °C (Haberkorn et al., 2015a) compared to compact, near-vertical bedrock (Gruber et al., 2004a; Hasler et al., 2011; Noetzli et al., 2007).

In order to assess contrasting influences of heterogeneous snow distribution on the ground thermal regime, the integration of the snow cover in distributed energy balance modelling of steep bedrock is necessary. The one-dimensional (1d) modelling approach used by Haberkorn et al. (2015b) to investigate the influence of the snow cover on near-surface rock temperature (NSRT) and the rock thermal regime demonstrated that the SNOWPACK model (Lehning et al., 2002a,b; Luetschg et al., 2003) is able to simulate the effect of a snow cover on rock temperature. However, to account for the complex micro-topography in rough rock walls and their influence on local shading effects, small-scale snow distribution and rock temperatures, a spatially distributed energy balance approach is necessary.

We therefore present a spatially distributed study on the influence of the snow cover on the surface energy balance and consequently on the rock thermal regime of a steep N–S oriented rock wall using the physics based 3d atmospheric and surface process model Alpine3D (Lehning et al., 2006). The spatially and temporally heterogeneous snow cover in such steep terrain (up to 85°) was provided to the model using a precipitation scaling approach. This was based on combining snow depth measurements from the on-site flat field automatic weather station (AWS) with the high resolution snow depth distribution data obtained using TLS. Hence, the challenge of integrating representative precipitation input (Imhof et al., 2000; Fiddes et al., 2015) and its redistribution by wind (Mott and Lehning, 2010), as well as avalanches (Gruber, 2007) is accounted for. High resolution (0.2 m) simulations are carried out, either providing snow cover distribution to the model or fully neglecting the presence of a snow cover to assess the potential error induced by neglecting the snow cover in steep rock face thermal modelling.

2. Study site

The Gemsstock mountain ridge (46° 36' 7.74" N; 8° 36' 41.98" E; 2961 m a.s.l.) is located on the main divide of the Western Alps, central Switzerland (Fig. 1a). Gemsstock is affected by both northerly and southerly airflows, resulting in enhanced orographic precipitation (for more information see Haberkorn et al. 2015a). The rocky ridge consists of Gotthard paragneiss and granodiorite, with veins of quartz. The site is at the lower fringe of mountain permafrost. Permafrost distribution is patchy in the north-west facing rock wall, whereas there is no permafrost in the south-east facing wall of the ridge (PERMOS, 2013).

This study focuses on a specific area on the north-west and south-east facing rocky flanks of the ridge (Fig. 1a), which are subsequently simply referred to as the N and S slopes. The 40 m high slopes are 40° to 70° steep, with vertical to overhanging (> 90°) sections (Fig. 1). The N facing scarp slope is intersected by a series of parallel joints dipping south-eastwards at 70° (Phillips et al., 2016). These joints form 0.3 to 3 m wide horizontal ledges within the NW facing rock wall and alternate with steep to vertical parts. In contrast, the S facing dip slope has a rather smooth rock surface. We investigate the 2 year study period between 1 September 2012 and 31 August 2014.

The Cryosphere Discuss., doi:10.5194/tc-2016-73, 2016
Manuscript under review for journal The Cryosphere
Published: 18 April 2016

3. Methods

3.1 Near-surface rock temperature (NSRT)

Maxim iButtons® DS1922L (Maxim Integrated, 2013) temperature loggers were used to measure NSRTs in 0.1 m deep boreholes at 2-hour intervals. After calibration in an ice-water mixture instrument accuracy was ±0.25 °C at 0 °C (for more information see Haberkorn et al. 2015b). To study the spatially variable thermal regime of the rock slopes, 30 of these temperature loggers were deployed in a linear layout over the N and S facing rock walls (Fig. 1) with a vertical spacing of approximately 3 m. However, data from 4 NSRT loggers (Table 1, Fig. 1) representing typical contrasting snow cover conditions in the N and S facing rock walls will be presented in detail here to validate and discuss the Alpine3D model results: logger N3 is located in a vertical sector near the top of the N facing rock wall, whereas logger N7 is located 12 m lower at the foot of this rock wall sector, close to a ledge. Pronounced daily NSRT amplitudes indicate that N3 was generally snow-free. Although logger N7 is located in 90° steep rock, a wide ledge 0.1 m below allows the accumulation of a thick snow cover in winter causing strong NSRT damping during the snow-covered period, as well as a zero-curtain in spring. On the S side of the ridge, logger R2 is in 58° steep rock 15 m above a ledge, whereas logger S9 is located in 70° steep terrain close to the gently inclined foot of a rock outcrop on the S facing rock wall. NSRT data indicate that R2 was generally snow-free and logger S9 was covered with a thick layer of snow in winter.

3.2 Terrestrial laser scanning (TLS)

TLS was carried out at Gemsstock for both the N and the S facing rock walls in summer using a Riegl *LPM-321* scanner to provide a high-resolution digital elevation model (DEM) of the snow-free rock walls. In addition, snow distribution and depth were measured at different times in the winter since 2012 using a Riegl *VZ6000* long-range laser scanner. A total of 4 high-resolution scans were carried out, two per winter. The high spatial and temporal variability of snow distribution and snow depths in the rock walls were determined by comparing the data to that obtained in the snow-free summer scans. To do this, the shortest distance from each terrain point to the point cloud at the snow surface was calculated with a point resolution of 0.2 m (Haberkorn et al. 2015a,b). The snow depth determined perpendicular to the surface were both more representative regarding their impact on ground temperatures (Haberkorn et al., 2015b) and more accurate (Sommer et al., 2015) than conventional vertical snow depths in extremely steep terrain. Parts of the NSRT measurement line and Alpine3D modelling domain were not visible in the laser scans due to blind areas behind ridges or rocky outcrops. The measurement error made using TLS for snow depth measurements is assumed to be ±0.08 m (Haberkorn et al., 2015b) and is therefore similar to other observations in steep rock (Sommer et al., 2015). Snow depths acquired from TLS were used as input data for the precipitation scaling approach discussed in detail in Sect. 3.3.3.

3.3 Distributed energy balance modelling

3.3.1 The Alpine3D model

The fully distributed physically based surface process model Alpine3D (Lehning et al., 2006, 2008; Kuonen et al., 2010) was used to simulate the influence of the heterogeneously distributed snow cover on the rock thermal regime of the Gemsstock ridge. The model is driven by meteorological data, which is pre-processed, as well as spatially interpolated and parametrized with the MeteoIO library (Bavay and Egger, 2014). A DEM and a land-use model are also required to run Alpine3D. In the setup used here Alpine3D consists of a 3d radiation balance model, which is based on the view factor approach to calculate short- and longwave radiation in complex terrain,

The Cryosphere Discuss., doi:10.5194/tc-2016-73, 2016
Manuscript under review for journal The Cryosphere
Published: 18 April 2016

including shortwave scattering and longwave emission from the terrain (Helbig et al., 2009). The 3d atmospheric processes are coupled to the 1d energy balance model SNOWPACK (Wever et al., 2014). The latter is based on the assumption that there is no lateral exchange in these media. The 3d snow drift module (Lehning et al., 2008) was not included in the simulations, although locally variable snow redistribution and snow erosion due to wind were observed at Gemsstock (Haberkorn et al., 2015a) and other rock walls (Wirz et al., 2011) because there is currently no model that convincingly reproduces 3d wind fields (Mott and Lehning, 2010) over extremely steep, heterogeneous rock walls. In addition the mass conserving computation of gravitational transport and deposition of snow (Bernhardt and Schulz, 2010; Gruber, 2007) is not included in simulations, although sloughing and avalanching were observed in the field (Haberkorn et al., 2015a) and have been suggested as the main process involved in the redistribution of snow in steep rock walls by Sommer et al. (2015). Therefore, we used measured TLS data to scale precipitation grids (Sect. 3.3.3) in order to represent the effects of snow redistribution on the snow cover distribution.

SNOWPACK simulates the temporal evolution of the vertical transport of mass and energy, as well as phase-change processes for a variety of layers within the seasonal snowpack and in the ground (Luetschg et al., 2003, 2008; Wever et al., 2015) for each single grid cell, solving the heat transport equation using a finite element method (Bartelt and Lehning, 2002). The albedo formulation for snow is calculated by a statistical model for seasonal snow in alpine terrain (Schmucki et al., 2014). A bulk Monin-Obukhov formulation is used to parameterize the latent and sensible heat fluxes. A Neumann boundary condition for the temperature equation is applied to simulate the net heat flux at the surface. The water flow in the snow and rock is solved using a simple bucket type approach, which is suitable for daily and seasonal time scales (Wever et al., 2014). The heat conduction equation is solved vertically (1d) in both the snow and ground, hence a constant upward ground heat flux is applied as the lower boundary condition.

3.3.2 Model setup

For this application the model was driven by meteorological data measured by the on-site AWS Gemsstock (2869 m a.s.l.), located at the foot of the northern rock slope (Fig. 1a). The AWS provided meteorological data during most of the investigation period 2012-2014. Measured air temperature, relative humidity, wind speed and direction, incoming short- and longwave radiation and (indirectly) snow depth were used as input data. Meteorological data and gaps were corrected according to Haberkorn et al. (2015b). The DEM is derived from the high-resolution TLS data at a grid resolution of 0.2 m and a domain size of 4460 m^2 (Fig. 1a). On the basis of the DEM, the rock layers of the SNOWPACK model were initialized with different layer temperatures based on measured borehole rock temperatures (Haberkorn et al., 2015b), depending on whether the grid cell was N or S facing. The ground is simulated to 20 m depth, divided into 24 layers of varying thickness ranging from 0.02 m at the surface to 4 m at the bottom of the substrate. The appropriate typical physical properties of the granodiorite bedrock were obtained from Cermák and Rybach (1982): the rock density is 2600 kg m^{-3}, the specific heat capacity is 1000 J $kg^{-1}K^{-1}$, the thermal conductivity is 2.8 W $m^{-1}K^{-1}$ on the S side and 1.9 W $m^{-1}K^{-1}$ on the N slope, as discussed in Haberkorn et al. (2015b). The rock albedo is assumed to be 0.15 and an aerodynamic roughness length of 0.002 m over snow is used for simulations. Down to 0.5 m depth the rock was assumed to be 99 % solid and 1 % pore space containing ice (N slope) or water (S slope) to account for near-surface fracture space. A solid content of 100 % was assumed between 0.5 m and 20 m depth. The geothermal heat flux is most likely negligible in the narrow, steep and complex Gemsstock ridge due to strong topographic

The Cryosphere Discuss., doi:10.5194/tc-2016-73, 2016
Manuscript under review for journal The Cryosphere
Published: 18 April 2016

(Kohl, 1999) and 3d thermal effects (Noetzli et al., 2007). The ground heat flux is therefore assumed to be 0.001 W m^{-2} at 20 m depth. This ensures a marginal impact of the lower boundary condition on the analysed rock thermal regime close to the surface. All high-resolution simulations were run in parallel mode on the same computer cluster as a 28 core process, requiring around 10 days for a two-year simulation. Simulations were also performed for coarser resolutions (1 m, 5 m) to analyse the loss of model accuracy for lower computational costs.

The Alpine3D output at grid points corresponding to the 30 NSRT locations have a temporal resolution of two hours, according to the time resolution of the measured validation data. A detailed point validation of modelled and measured snow depth (derived by TLS) and NSRT data was therefore feasible. Errors made in modelling the distributed ground thermal regime in steep rock walls were assessed statistically for both the snow-covered and the snow-free approach using the mean bias error (MBE) and the correlation of determination (r^2).

3.3.3 Precipitation scaling

The bias involved in driving precipitation from a single AWS (Grünewald and Lehning, 2011) in combination with a snow redistribution routine applied for moderately steep terrain, such as that developed by Winstral et al. (2002) were found to be insufficient to model the snow cover in steep rock walls (not shown). To exploit the availability of high resolution spatially explicit snow depth distribution provided by TLS for driving the Alpine3D model, a precipitation scaling algorithm was applied. Alpine3D only uses precipitation as input data. As precipitation data was not available for Gemsstock, precipitation was calculated from the snow depth measured at the AWS using a stand-alone SNOWPACK simulation. By using the snow depth driven mode of the SNOWPACK model, the snow depth measurements were used to determine the timing and amount of snowfall by interpreting increases in snow depth as snowfall according to Lehning et al. (1999). To complete the resulting precipitation series, summer liquid precipitation was integrated from the nearby MeteoSwiss AWS Gütsch (2287 m a.s.l., 6 km north of Gemsstock; Haberkorn et al. 2015b). The ratio between measured snow depth at the AWS and the distributed snow depth measured by TLS was used to scale the precipitation time series derived from the SNOWPACK simulation for the AWS Gemsstock onto the DEM. However, data gaps in the TLS (Fig. 2b,c) lead to data gaps in the precipitation scaling grid. For grid cells lacking a precipitation scaling factor, the precipitation measured at the AWS Gemsstock was assumed, resulting in erroneously modelled snow depths and ground temperatures at these locations. The Alpine3D grid output with incomplete TLS data was therefore extracted to avoid errors in the analysis.

Precipitation scaling and an Alpine3D model run were carried out for each of the four TLS. However, the modelled snow depth and NSRT data coincided best with validation data when using scaled precipitation and snow depth data based on the TLS of 11 December 2013 (Fig. 2b, c). The reason for this is unclear but early winter TLS best represent winter snow fall events. TLS carried out in spring already contain processes modelled by Alpine3D, such as ablation. Henceforth, the modelled results analysed and discussed here are based solely on the TLS of 11 December 2013. This is justified by annually recurring micro-topography driven snow distribution and snow depth patterns observed in steep rock walls by Wirz et al. (2011), Sommer et al. (2015) and Haberkorn et al. (2015a). We refer to this method as precipitation scaling, which provides grids of spatially distributed precipitation amounts for Alpine3D input.

In order to perform a sensitivity analysis to assess and discuss the bias made while neglecting snow, the rock thermal regime was additionally modelled for snow-free conditions. To do this, precipitation data was forced to

The Cryosphere Discuss., doi:10.5194/tc-2016-73, 2016
Manuscript under review for journal The Cryosphere
Published: 18 April 2016

be zero. Alpine3D simulations were thus carried out for two contrasting settings: snow-covered and snow-free conditions.

3.3.4 Surface energy balance modelling

The energy balance is one of the most important input factors influencing the ground thermal regime. The surface energy balance is determined by the exchange of energy between the atmosphere and the snowpack or the ground. The energy flux Q_{melt} (Eq. 1) available for warming and melting or cooling and freezing of the snowpack or the ground is calculated as the sum of all energy balance components [W m^{-2}] at the respective surface (Armstrong and Brun, 2008). In Alpine3D energy fluxes are considered positive when directed towards the snowpack surface (energy gain).

$$Q_{melt} = Q_{net} + Q_{sensible} + Q_{latent} + Q_{rain} + Q_{ground} \quad (1)$$

Where Q_{net} is the sum of the net fluxes of short- and longwave radiation, $Q_{sensible}$ and Q_{latent} are the turbulent fluxes of sensible and latent heat through the atmosphere, Q_{rain} is the rain energy flux and Q_{ground} is the 1d conduction of heat into the ground.

4 Results

4.1 Spatial snow cover variability

4.1.1 Measured snow cover variability

Similar annual and inter-annual patterns of snow depth and snow distribution can be observed using TLS, whereas inter-annual variations in snow depth in adjacent flat terrain can be derived from the AWS data (Fig. 2a). In 2012-2013 a 4.5 m thick snowpack accumulated at the AWS. In contrast, snow depths were on average 1 m lower at both the AWS and NSRT logger locations in 2013-2014, resulting in snow disappearance up to 4 weeks earlier. The variability of snow depth distribution was high at the local rock wall-scale. Steep to vertical areas far above ledges or areas close to the ridge were usually snow-free, as was the case for the N3 and R2 loggers (Fig. 2b-d, Table 2). However, areas accumulating a thick snow cover can exist in the immediate vicinity of snow-free areas due to strongly varying micro-topographic effects. Locations close to the foot of the rock wall and steep areas just above flat ledges accumulated mean snow depths up to 3.5 m (Fig. 2b, c). The snow cover was more homogeneous and thicker on the smoother S slope than on the steeper and rougher N slope. Hence, snow cover onset and disappearance, as well as snow distribution strongly varied within and across the N and the S facing rock walls. At logger N7, measured snow depths were around 1 m at the beginning of both winters, whilst snow depths varying between 1.5 and 2 m were measured at S9 in the S slope (Fig. 2a).

4.1.2 Scaled snow cover variability

The scaled snow depths for 11 December 2013 and their distribution were very similar to the corresponding TLS data (Fig. 2b, c), with an r^2 value of 0.94 and a MBE of -0.002 m averaged over the entire model domain. Errors were slightly higher in the heterogeneous N slope than in the smoother S slope.

To assess the sum of uncertainties induced by the combined errors of TLS (±0.08 m), which were inherited in the precipitation scaling approach and the errors of the precipitation scaling approach itself, a MBE analysis was performed for each NSRT logger accumulating snow (error bars in Fig. 2a). Scaled snow depth accuracy was

The Cryosphere Discuss., doi:10.5194/tc-2016-73, 2016
Manuscript under review for journal The Cryosphere
Published: 18 April 2016

worst in areas with a strongly heterogeneous snow distribution. Hence, the error at the heterogeneous location of N7 (±0.3 m) was twice as large as that at the smoother location of S9.

4.1.3 Modelled snow cover variability

The evaluation of snow depth distribution modelled using Alpine3D against data from four independent TLS revealed an accurately reproduced snow distribution (r^2 = 0.95), while snow depth differences were in the range of +0.5 m to -1 m, shown in Fig. 2f on 11 December 2013. However, snow depths mainly varied by ±0.5 m. In the S facing slope modelled snow depths are often underestimated, whilst in the N slope they are mostly overestimated.

In Fig. 2a the evolution of modelled snow depths for two selected points within both the N (N7) and the S (S9) facing slopes are shown. Here, NSRT data (Fig. 3b,c) confirmed an accurately modelled timing of snow cover onset and disappearance (Table 2). Snow accumulated at both loggers for 8 to 9 months of the year. TLS snow depths (dots in Fig. 2a) are used to validate the modelled winter snowpack on the dates of TLS campaigns. At the shaded N7 location, the measured and modelled snow depths fit reasonably well in both winters 2012-2013 and 2013-2014. Modelled snow depths are overestimated by up to 0.2 m in winter, whilst in early summer they are underestimated by 0.6 m. This most likely results from excess modelled insolation in this north-west facing slope (see Sect. 5.1). Increased differences between measured and modelled snow depths up to 1 m were observed in the S facing slope due to inadequate description of snow settlement (see Sect. 5.1).

4.2 NSRT variability at selected points

The measured and simulated NSRT evolution in 0.1 m depth at four selected NSRT logger locations with differing snow conditions (Table 1) in both the N and the S facing rock walls are illustrated in Fig. 3. A bias assessment was performed between measured and modelled NSRT for each individual location for both the snow-free and the snow-covered case (Table 2, Fig. 4).

4.2.1 Measured NSRT variability

At locations favouring the accumulation of a thick snowpack the NSRT evolution was strongly controlled by snow for around 9 months of the year in both the N (N7 in Table 1, Fig. 3b) and the S (S9 in Table 1, Fig. 3c) facing rock walls. After the onset of the continuous snow cover in October the rock surface was partly decoupled from atmospheric influences. In the N facing slope measured NSRT oscillations were damped, but continuously decreased down to -4 °C and thus clearly showing a permafrost signal at this location, while in the S facing slope measured NSRT remained close to 0 °C. Although the timing of snow cover onset and disappearance were similar in both the N and the S facing slope (Table 2), the start of the zero curtain period was delayed by up to 1.5 months in the N facing slope (beginning of May). Mean annual near-surface rock temperature (MANSRT) differences were only up to 2.4 °C between the N (N7) and the S (S9) facing locations due to the thick snow cover. The snow cover onset during both years was similar, while the onset of the zero curtain period was two weeks earlier and the snow disappearance up to 4 weeks earlier (mid-June) in 2013-2014. The latter caused up to 0.4 °C warmer MANSRT in 2013-2014 than in the previous year due to the snow-free conditions during the weeks with most intense solar radiation (mid-June to mid-July).

At NSRT locations lacking snow, NSRTs closely followed air temperature in the shaded N face (N3 in Table 1, Fig. 3d) while pronounced daily NSRT amplitudes up to 10 °C could be observed at sun-exposed locations (R2

The Cryosphere Discuss., doi:10.5194/tc-2016-73, 2016
Manuscript under review for journal The Cryosphere
Published: 18 April 2016

in Table 1, Fig. 3e) during the whole investigation period. The topography driven MANSRT difference between the N (N3) and the S (R2) facing locations was 3.6 °C. Similar to the snowy locations, the MANSRT was up to 0.6 °C higher here in 2013-2014 compared to 2012-2013, but here induced by the 0.9 °C warmer mean annual air temperature in 2013-2014 (Table 3).

4.2.2 Modelled NSRT variability

The modelled NSRTs and their temporal evolution are in good accordance with the measured ones at locations accumulating a thick snow cover (Fig. 4a, d) in both the N (N7) and the S (S9) facing slopes. Daily variations between measured and modelled NSRT are below 4 °C in summer (dT in Fig. 3b, c). During the snow-covered period measured and modelled NSRT and therefore MANSRT are in auspicious accordance in the S facing slope (MBE -0.15 °C), while measured NSRT, as well as MANSRT are on average 1.2 °C colder than modelled ones in the N facing slope (Figs. 3b, 4a, Table 2). However, in both the shaded and sun-exposed rock slopes the modelled timing of the snow cover onset, the zero curtain period and the snow disappearance was similar to the measured ones (Table 2).

At logger locations lacking snow (N3, R2 in Table 2, Fig. 3d, e) pronounced daily NSRT amplitudes were measured and modelled during the whole investigated period (up to 12 °C). Measured and modelled NSRT evolution was in good accordance (r^2 up to 0.92, Fig. 4c, f). However, the MBE between measured and modelled NSRT was up to -2.0 °C for both the N and the S facing rock slopes, indicating always colder modelled NSRT conditions. The largest differences between measured and modelled daily NSRT amplitudes were mainly observed during winter in both rock walls.

4.2.3 Modelled NSRT variability with forced snow-free conditions

Although measured NSRT confirm the accumulation of a thick snow cover at the locations N7 and S9, NSRT were also modelled here assuming snow-free conditions. Modelled NSRT evolutions of N7 and S9 were similar to the snow-free locations of N3 and R2, discussed previously. Modelled NSRT oscillations were pronounced during the whole study period. MANSRTs were up to -2.5 °C in the shaded and up to 1.8 °C in the sun-exposed slopes. Therefore, modelled MANSRT for snow-free conditions were up to 3.7 °C colder in the shaded and up to 1.6 °C colder in the sun-exposed rock wall locations, when comparing to measured and modelled MANSRT accumulating an insulating snow cover. The apparent deviations between measured and modelled NSRT caused the r^2 to decrease (Fig. 4b,e) and the MBE to increase (Table 2).

4.3 MANSRT variability in the rock walls

At the 30 NSRT locations measured and modelled NSRT data were used to calculate MANSRT means, as well as the variability (standard deviation) of MANSRT within the individual N and S facing rock walls. Modelled MANSRT were also averaged for both slopes over the entire model domain.

4.3.1 Measured MANSRT variability

Comparing the MANSRT averaged over the entire N facing rock wall (up to -0.7 °C) with the MANSRT of the entire S facing rock wall (up to 2.9 °C) resulted in a MANSRT difference of 3.6 °C. This was not as pronounced as expected in steep rock due to the accumulation of a thick snow cover at most locations.

The Cryosphere Discuss., doi:10.5194/tc-2016-73, 2016
Manuscript under review for journal The Cryosphere
Published: 18 April 2016

The measured small-scale variability of MANSRT within the individual N and S facing rock walls was greater in 2012-2013 (Fig. 5, Table 3). Smaller MANSRT variability in 2013-2014 resulted from two compensating effects: In 2013-2014 both winter- and mean annual air temperatures were warmer, causing MANSRTs at snow-free locations to increase by around 0.6 °C. In contrast, MANSRTs at snow-covered locations decreased by up to 0.4 °C due to the absence of a sufficiently insulating snow cover in the beginning of winter 2013-2014 (Haberkorn et al., 2015a), which resulted in effective ground heat loss at snow-covered locations in the N slope.

4.3.2 Modelled MANSRT variability

The modelled and measured MANSRTs and their annual trends coincide well in the N facing slope (Table 3). However, modelled MANSRT variability was higher (Table 3, Fig. 5) than measured data. This resulted from a combination of artificially low modelled MANSRT at locations lacking snow and artificially high modelled MANSRT at snow-covered locations during winter.

In the S facing slope, modelled MANSRT was on average 2 °C for both 2012-2013 and 2013-2014, which is up to 1 °C colder than measured MANSRT. The underestimation of modelled NSRT mainly occurred in summer. Therefore, the difference between modelled MANSRT across the N and the S facing slopes was only up to 2.5 °C.

4.3.3 Modelled MANSRT variability with forced snow-free conditions

Modelled MANSRT of snow-free simulations were up to -2.9 °C within the N facing slope and up to 1.3 °C within the S slope and therefore around 2 °C colder compared to snow-covered conditions. In the absence of a snow cover, the MANSRTs were only controlled by aspect and slope dependent effects (air temperature, solar radiation), inducing smaller modelled MANSRT variabilities within the individual rock walls (Fig. 5).

Across the individual N and S facing slopes modelled MANSRT differences for snow-free conditions were only up to 3.4 °C and therefore not as pronounced as would be expected in steep slopes lacking snow. However, it can be assumed that modelled MANSRT differences between the N and the S slopes lacking snow were up to 4.4 °C, because MANSRT were 1 °C too cold modelled in the S face (Fig. 5).

4.3.4 Modelled spatial distribution of MANSRT variability

Modelled MANSRT for each grid cell of the entire N and S slope (not just at selected NSRT locations) are shown in Fig. 6 for the year 2012-2013. MANSRT were warmest at the foot of both rock walls and gradually decreased from flat to steep areas due to both snow depth decrease (assuming snow-covered conditions) and low insolation in the N slope (assuming snow-free conditions). Additionally MANSRT at locations shadowed by rock outcrops or in rock dihedrals were colder compared to their surrounding areas (arrows in Fig. 6a, b). The modelled MANSRT were controlled by the snow cover, resulting in up to 1.9 °C higher MANSRT (Table 3, Fig. 6e, f) than for snow-free conditions.

4.4 Modelled surface energy balance at selected points

The dominant driving factors contributing to the modulating influence of the snow cover on the rock thermal regime close to the surface (0.1 m depth) can be assessed by analysing the surface energy balance. In Fig. 7 modelled monthly means of each individual energy transfer term are shown for a sun-exposed (S9) and a shaded location (N7) with thick snow covers. The varying importance of the modelled energy fluxes are discussed for

The Cryosphere Discuss., doi:10.5194/tc-2016-73, 2016
Manuscript under review for journal The Cryosphere
Published: 18 April 2016

snow-covered and snow-free conditions in the steep rock walls. The terms of the energy budget were previously defined.

4.4.1 N facing slope

At the steep, shaded location N7 (Fig. 7a) the modelled mean monthly energy balance was strongly influenced by local micro-topographic effects (steep rock, thick snow cover). From October to March almost no solar radiation was received and energy was lost by surface radiation emission. The resulting net radiation flux Q_{net} was therefore negative. However, energy was transferred towards the surface by convection of sensible heat $Q_{sensible}$ from the warmer air to the colder snow surface, which was in the same order of magnitude as Q_{net}. In contrast the latent heat flux Q_{latent} was low. Q_{ground} was low due to the insulating snowpack and positive, since the measured permafrost signal could not be reproduced by the model. Q_{rain} was negligibly small compared with other fluxes and will not be discussed further here. Between April/May and September more radiation was absorbed than reflected and emitted, causing a positive Q_{net}. The snowmelt energy flux Q_{melt} affected the energy balance between April and June, and any energy surplus was used for melt. The positive surface energy balance first resulted in a heating of the snowpack to 0 °C followed by melt, which corresponded to the zero curtain period of measured and modelled NSRTs (Fig. 3b). Q_{ground} was still negligible during the ablation period.

In contrast to the radiation budget of the snow-covered steep N facing location of N7, the monthly evolution of the modelled surface energy balance components for snow-free conditions (Fig. 7b) differed strongly. Q_{net} increased uniformly from negative values in winter to maximum values in summer. During the months with low solar elevation (November-January) the energy loss by Q_{net} was smaller on bare rock due its lower albedo and emissivity. The sensible heat flux towards the surface was smaller for snow-free conditions, but the ground heat released in fall and winter was increased due to the absence of snow. Q_{ground} was directed into the rock during spring and summer. From March to July the energy gained by Q_{net} was considerably higher compared to the snow-covered case due to the absence of snow, which was mainly compensated by $Q_{sensible}$.

4.4.2 S facing slope

Although the monthly evolution of the energy fluxes in the steep, snow-covered and sun-exposed location of S9 (Fig. 7c) were similar to those of N7, variations in the magnitude of the fluxes were observed. During November and March energy was lost by Q_{net} and Q_{latent}. However, Q_{net} was less negative than in the N face due to strong insolation in winter. During the snowmelt period from April to June/July the energy budget was positive. However, the magnitudes of the fluxes were smaller in the slightly less inclined S slope compared to the steeper north-west exposed location of N7.

The temporal evolution of the modelled energy fluxes at locations lacking snow (Fig. 7d) varied strongly. Q_{net} was positive throughout the whole year, displaying a sinusoidal cycle with minimum values in winter und maxima in summer. The strong Q_{net} input in winter is caused by stronger direct solar radiation input on steep S facing slopes due to the low solar elevation and perpendicular angle of incoming solar radiation.

5 Discussion

5.1 Model uncertainties

Limitations in the quality of snow cover, energy balance and rock temperature simulations were introduced by uncertainties in the input data (see previous sections), as well as the adequacy of the process representation in the

Alpine3D model. Some physical processes, such as water flow on the rock surface and along fractures (Phillips et al., 2016) or the heterogeneous wind field in extremely steep terrain, are currently insufficiently represented by our model setup.

An accurately modelled snow cover evolution and its spatial patterns are crucial to correctly model the ground thermal regime (Fiddes et al., 2015; Hoelzle et al., 2001; Stocker-Mittaz et al., 2002). The precipitation scaling algorithm used here implicitly assumes a mean constant snow density (i.e. the snow depth scales linearly with the precipitation amount) calculated for snow depths at the AWS location. However, due to precipitation scaling snow depths in the rock walls vary compared to the snow depth modelled at the AWS and thus will settle differently due to a non-linear snow cover settling. Differences in settling calculated at the AWS and for the grid points in the Alpine3D model domain therefore cause snow depth errors. However, on the basis of measured NSRT it is evident that a realistically modelled snow cover duration over the winter is more important than accurately modelled snow depths at certain points in time. This agrees with the findings of Marmy et al. (2013) and Fiddes et al. (2015). The overall performance of Alpine3D modelling snow depths in steep slopes in the current setup thus provides useful improvements compared to traditional snow modelling techniques in steep rock (e.g. Boeckli et al., 2012a,b; Fiddes et al., 2015; Gruber et al., 2004a; Noetzli et al., 2007). Further, we found that the apparent insulation by snow was too strong in the simulations, which has two possible explanations: (i) Snow thermal conductivity is too low in the model. (ii) Lateral heat fluxes between snow-covered and snow-free rock portions, which lead to stronger cooling below snow pixels than simulated with the 1d model. An additional reason is possibly the lower boundary condition of a constant upward heat flux, which is insufficient to describe the complex 3d heat flow occurring in steep, narrow ridges (Noetzli et al., 2007). Modelled NSRT and consequently MANSRT were therefore positively biased during the snow-covered period in the rough N facing slope and thus the measured permafrost signal (Fig. 3b) could not be reproduced. While assuming predominately 1d vertical heat conduction in the snow and ground, a part of the energy balance is only poorly described or missing (Noetzli et al., 2007), especially in the steep heterogeneous N facing rock wall. For example effective ground heat loss in autumn 2013-2014 was observed at exposed locations due to an initially thin snow cover, while adjacent locations covered with thick snow showed this NSRT cooling too (Haberkorn et al., 2015a). The NSRT cooling in 2013-2014 was successfully modelled for individual locations, but not the heat exchange between grid cells, although the fine resolution of the model domain would provide the basis to account for such variable topographic influences. In contrast in the homogenous S facing slope modelled NSRT supported the validity of the 1d heat conduction assumption since a continuous, smooth snowpack was an effective barrier to heat loss from the ground to the air (Fig. 3c). Difficulties in partitioning the measured incoming shortwave radiation in a direct and diffuse component, particularly for low sun angles, may explain the stronger modelled net radiation for snow-free conditions in the shaded (Fig. 7b, Table 1) than in the sun-exposed slope (Fig. 7c). Additionally, the underestimation of modelled daily NSRTs, especially at steep S facing locations lacking snow (R2 in Fig. 3e) in summer is apparent. A likely explanation is that both air temperature and wind speeds in the rock wall are poorly represented by the AWS measurements and therefore turbulent flux simulations are erroneous. This resulted in negatively biased modelled MANSRTs, although the timing of the snow cover duration was accurately modelled in both the N and the S facing slopes.

MBE analysis suggest an average MBE of -0.2 °C in shaded and up to -1 °C in sun-exposed rock walls while applying Alpine3D in steep rough rock to simulate NSRT.

The Cryosphere Discuss., doi:10.5194/tc-2016-73, 2016
Manuscript under review for journal The Cryosphere
Published: 18 April 2016

5.2 Impacts of snow in rock walls

Meteorological conditions and topographic properties like slope angle, aspect, surface roughness (Gruber et al., 2004b; Noetzli et al., 2007) and local shading effects (Mott et al., 2011) control the surface energy balance and their annual variations in rock wall sectors lacking snow. Changes of local conditions at the rock surface due to the accumulation of a snow cover modify the importance of influencing factors on the ground energy balance (Hoelzle et al., 2001). Exchanges between the atmosphere and the rock were still obvious. This is attributed to a strong thermal interaction of micro-topography and micro-climate between adjacent snow-covered and snow-free locations and consequently to the substantial influence of lateral heat fluxes near the surface. These 2d heat fluxes were reported by Gruber et al. (2004c) and Wegmann et al. (1998) for differently exposed mountain sites lacking snow, by Noetzli et al. (2007) in the ground of convex topography, and by Mittaz et al. (2000) due to the presence of coarse blocks. Hence, it can be estimated that lateral heat fluxes in steep rock are also caused by the strongly variable terrain and snow cover distribution, which was neglected by these authors.

In order to estimate the error possibly made by neglecting the snow in steep bedrock in permafrost distribution modelling, Alpine3D was also used to simulate for snow-free conditions. A prominent warming effect of the snowpack on MANSRT in both the entire N and S facing steep rock walls were modelled at the point- and the local rock wall-scale (Table 2, 3) and support the observations by Haberkorn et al. (2015a). Modelled MANSRT differences between snow-covered and snow-free conditions were higher in the shaded N slope (up to 2 °C), while MANSRT differences were around 1.4 °C in the sun-exposed slope. In the S slope the smaller differences between snow-covered and snow-free conditions were due to the prevention of the rock from heating up despite the large insolation in spring and early summer (Fig. 7c, d). At locations lacking snow the excessive radiation input in early summer cannot compensate the effective ground heat loss in winter. The assumption made by Magnin et al. (2015) and Hasler et al. (2011), who supposed a cooling effect of a long lasting snow cover due to the prevention of the rock surface from radiation influences for the months with most intense insolation in sun-exposed rock walls is therefore questioned. It is proven that both net radiation (Fig. 7) and the snow cover are the key factors driving ground temperatures and determine whether permafrost is present or not in steep, rough rock walls, which was already proposed in moderately inclined terrain by Hoelzle et al. (2001). In steep S facing mountain ridges up to 3000 m a.s.l. permafrost is most likely absent independent of the evolution of a thick snow cover. In contrast in steep rugged N facing rock walls the accumulation of a thick snow cover prevents a continuous permafrost distribution, while permafrost would most likely be present assuming a lack of snow. We suggest that in recent permafrost distribution assessments based on energy balance (Fiddes et al., 2015) or statistical modelling (Boeckli et al., 2012a,b) in the European Alps mean annual rock surface temperatures were modelled too cold by 2 °C in steep N facing bedrock and up to 1 °C in steep S facing bedrock due to neglecting of snow. The implementation of 3d advective heat fluxes influencing already the rock surface and not just ground temperatures at depth (Noetzli et al., 2007) will be a crucial further step for modelling the ground thermal regime in steep bedrock.

5.3 Influences of grid resolution

The model performance was tested at different scales ranging from 0.2 m, 1m to 5 m. At locations with rough micro-topography the loss of information was big due to the aggregation of the initial DEM (0.2 m resolution) to 1 m and 5 m. Slope angles were only sampled <70° (1 m resolution) and <60° (5 m resolution), while in reality the rock was vertical. Aspects were displaced by up to 90°. This has a strong effect of the precipitation scaling

and the modelled energy- and mass balance of the rock walls. Shortwave incoming radiation was inadequately modelled at locations with strongly varying micro-topography. However, on a monthly basis, errors in net radiation were smoothed. In both the N and the S facing rock walls modelled NSRTs confirm that a grid resolution of 1 m is acceptable to accurately model the snow cover and ground surface temperatures in steep rugged rock faces. The decrease in computational time by reducing the grid resolution from 0.2 m to 1 m, is significant (25 times smaller). Additionally, a DEM resolution of 1 m is considered to be precise enough to detect ledges within the rock face, which are essential for snow accumulation in steep rock (Haberkorn et al., 2015a; Sommer et al., 2015). At a resolution of 5 m the loss of topographic, as well as accurate snow depth information is huge and consequently snow distribution and the rock thermal regime were inadequately modelled in such complex terrain.

Mismatches of scaling issues in distributed permafrost modelling arise often while validating the model results based on grids of 10s - 100s of meters to point measurements (e.g. Gubler et al., 2011; Gupta et al., 2005; Schlögel et al., 2016). Here a point to point validation of NSRTs was performed at a dense network of 30 NSRT measurement locations. Additionally TLS derived snow depth grids were compared to modelled snow depth grids at TLS recording date both with a resolution of 0.2 m. The data validation revealed similar MANSRT and MBE for both, the point- and the rock wall-scale implying that fewer validation locations in the rock walls are sufficient. The point validation to data with 1 m resolution is reasonable, while 5 m resolution is already insufficient.

6 Conclusions

The potential to model the strongly heterogeneous snow cover and its influence on the rock thermal regime on rugged, steep rock walls has been studied here. The results were obtained using the spatially distributed physics-based model Alpine3D in combination with a precipitation scaling approach. Modelling the impact of snow on ground temperatures in steep rock revealed potential errors made in recent ground temperature modelling when neglecting the evolution of the snow cover in terrain exceeding 50°.

Alpine3D simulates near-surface rock temperatures and snow depth in the heterogeneous terrain accurately. The correction of winter precipitation input using a precipitation scaling method based on TLS greatly improves simulations of snow distribution and duration and thus of the rock thermal regime. Remaining errors in rock temperature simulations are explained by missing lateral heat fluxes in the rock, inadequate snow settlement and by errors due to shortwave radiation and wind interpolation, which are very complex in such terrain.

The fine-scale resolution of the model domain (0.2 m) and of the validation data allow to consider the strongly varying micro-topography occurring in the rock walls, and thus the accumulation of a heterogeneously distributed snow cover. An intensive thermal interaction of the micro-topography and micro-climate, especially between adjacent snow-covered and snow-free locations causes lateral heat fluxes near the surface which strongly influence the spatially varying NSRTs.

A strong warming of MANSRT in both the shaded and sun-exposed steep rock walls induced by a thick long lasting snow cover were measured and modelled. Thus MANSRT increased by 2 °C in the shaded and 1 °C in the sun-exposed rock wall while comparing snow-covered to snow-free conditions. As snow reduces ground heat loss in winter, it has an overall warming effect on both N and S facing rock walls despite the fact that it provides protection from solar radiation in early summer.

The model performance was tested at different scales ranging from 0.2 m to 5 m. A DEM resolution of 1 m is detailed enough to detect the strongly variable micro-topography in steep, rugged rock walls and hence a grid resolution of 1 m is adequate to accurately model the snow cover and rock surface temperatures.

7 Outlook

The observations and model results discussed here are from an individual site with specific characteristics. In future, additional rock faces with diverse characteristics and climates should be investigated. The precipitation scaling method presented here is currently only valid at the site-scale, but can potentially also rely on satellite imagery or airborne laser scan data to enable snow depth scaling for larger areas. Correcting for different snow settlement rates due to different snow depths will be a feasible improvement of snow depth simulations. Further improvements can be expected when both wind fields in steep terrain and lateral heat fluxes will be considered in the Alpine3D model. While the generation of wind fields over steep slopes is an unsolved challenging issue, the 3d character of heat flow in steep ridges can be addressed, while coupling the modelled surface energy balance to a ground model representing 3d heat flow in the rock. This will likely allow to model an accurate evolution of ground temperatures and potential disposition for slope instability. Although ground temperature modelling over larger areas, such as the entire Alps, is not feasible at such high resolution due to high computational effort, our site specific approach has demonstrated the potential to reveal temperature variations for different snow cover conditions and to discuss limitations of permafrost models running at coarse scales. Climate change impact studies critically depend on the small-scale variability at the atmosphere-surface interface. This physically based approach can be used to study the long-term effect of a changing climate on rock temperatures and permafrost distribution.

8 Data availability

The data is available on request from WSL Institute for Snow and Avalanche Research SLF. The model used is online available at http://models.slf.ch/.

9 Author contribution

A. Haberkorn and M. Phillips designed the measurement set-up, carried out the measurements and analysed the data. R. Kenner was responsible for terrestrial laser scanning and analysis of this data. M. Lehning, N. Wever and M. Bavay developed the Alpine3D model code. Additionally N. Wever developed the precipitation scaling approach. A. Haberkorn performed the simulations and prepared the manuscript with contributions from all co-authors, including energy balance analyses by M. Hoelzle.

10 Acknowledgements

This project is funded by the Swiss National Science Foundation (DACH Project no. 200021E-135531). We thank our project partners M. Krautblatter, D. Dräbing and S. Gruber, as well as H. Rhyner who was responsible for safety in the field. We acknowledge preparation and support of fieldwork by Carlo Danioth and Team at Gemsstock, the SLF Electronics, IT and Mechanics team, M. Keller, M.O. Schmid, L. Dreier, M. Sättele and F. Stucki. For constructive input W. Steinkogler, J. Caduff-Fiddes and J. Noetzli are thanked.

References

Armstrong, R.L., and Brun, E. (eds.): Snow and Climate: Physical Processes, Surface Energy Exchange and Modeling, Cambridge University Press, Cambridge, 256 pp, 2008.

Bartelt, P., and Lehning, M.: A physical SNOWPACK model for the Swiss avalanche warning: Part I: numerical model, Cold Reg. Sci. Technol., 35, 123-145, doi:10.1016/S0165-232X(02)00074-5, 2002.

Bavay, M., and Egger, T.: MeteoIO 2.4.2: a preprocessing library for meteorological data, Geosci. Model Dev., 7, 3135-3151, doi:10.5194/gmd-7-3135-2014, 2014.

Bernhard, L., Sutter, F., Haeberli, W., and Keller, F.: Processes of Snow/Permafrost-Interactions at a High-Mountain Site, Murtèl/Corvatsch, Eastern Swiss Alps, In: Lewkowicz, A.G., and Allard, M. (eds), Proceedings of the 7th International Conference on Permafrost, Collection Nordicana, 55, Université Laval, Yellwoknife, Canada, 35-41, 1998.

Bernhardt, M., and Schulz, K.: SnowSlide: A simple routine for calculating gravitational snow transport, Geophys. Res. Lett., 37, L11502, doi:10.1029/2010GL043086, 2010.

Blöschl, G., and Kirnbauer, R.: An analysis of snow cover patterns in a small alpine catchment, Hydrol. Process., 6, 99-109, doi:10.1002/hyp.3360060109, 1992.

Boeckli, L., Brenning, A., Gruber, S., and Noetzli, J.: A statistical approach to modelling permafrost distribution in the European Alps or similar mountain ranges, Cryosphere, 6, 125-140, doi:10.5194/tc-6-125-2012, 2012a.

Boeckli, L., Brenning, A., Gruber, S., and Noetzli, J.: Permafrost distribution in the European Alps: calculation and evaluation of an index map and summary statistics, Cryosphere, 6, 807-820, doi:10.5194/tc-6-807-2012, 2012b.

Cermák, V. and Rybach, L.: Thermal conductivity and specific heat of minerals and rocks, In: Angeneister, G. (ed.), Landolt-Börnstein Zahlenwerte und Funktionen aus Naturwissenschaften und Technik, Neue Serie, Physikalische Eigenschaften der Gesteine, Springer, Berlin, 305-343, 1982.

Davies, M.C.R., Hamza, O., and Harris, C.: The Effect of Rise in Mean Annual Temperature on the Stability of Rock Slopes Containing Ice-Filled Discontinuities, Permafr. Periglac. Process., 12, 137-144, doi:10.1002/ppp378, 2001.

Endrizzi, S., Gruber, S., Dall'Amico, M., and Rigon, R.: GEOtop 2.0: simulating the combined energy and water balance at and below the land surface accounting for soil freezing, snow cover and terrain effects, Geosci. Model Dev., 7, 2831-2857, doi:10.5194/gmd-7-2831-2014, 2014.

Fiddes, J., Endrizzi, S., and Gruber, S.: Large-area land surface simulations in heterogeneous terrain driven by global data sets: application to mountain permafrost, Cryosphere, 9, 411-426, doi:10.5194/tc-9-411-2015, 2015.

Fischer, L., Kääb, A., Huggel, C., and Noetzli, J.: Geology, glacier retreat and permafrost degradation as controlling factors of slope instabilities in a high-mountain rock wall: the Monte Rosa east face, Nat. Hazards Earth Syst. Sci., 6, 761-722, doi:10.5194/nhess-6-761-2006, 2006.

Gruber, S.: A mass-conserving fast algorithm to parameterize gravitational transport and deposition using digital elevation models, Water Resour. Res., 43, W06412, doi:10.1029/2006WR004868, 2007.

Gruber, S.: Derivation and analysis of a high-resolution estimate of global permafrost zonation, Cryosphere, 6, 221-233, doi:10.5194/tc-6-221-2012, 2012.

Gruber, S., and Haeberli, W.: Permafrost in steep bedrock slopes and its temperature-related destabilization following climate change, J. Geophys. Res., 112, F02S18, doi:10.1029/2006JF000547, 2007.

Gruber, S., and Hoelzle, M.: Statistical Modelling of Mountain Permafrost Distribution: Local Calibration and Incorporation of Remotely Sensed Data, Permafr. Periglac. Process., 12, 69-77, doi:10.1002/ppp374, 2001.

Gruber, S., Hoelzle, M., and Haeberli, W.: Rock-wall Temperatures in the Alps: Modelling their Topographic Distribution and Regional Differences, Permafr. Periglac. Process., 15, 299-307, doi:10.1002/ppp.501, 2004a.

Gruber, S., Hoelzle, M., and Haeberli, W.: Permafrost thaw and destabilization of Alpine rock walls in the hot summer of 2003, Geophys. Res. Lett., 31, L13504, doi:10.1029/2004GL020051, 2004b.

Gruber, S., King, L., Kohl, T., Herz, T., Haeberli, W., and Hoelzle, M.: Interpretation of Geothermal Profiles Perturbed by Topography: the Alpine Permafrost Boreholes at Stockhorn Plateau, Switzerland, Permafr. Periglac. Process., 15, 349-357, doi:10.1002/ppp.503, 2004c.

Gruber Schmid, U., and Sardemann, S.: High-frequency avalanches: release area characteristics and run-out distances, Cold Reg. Sci. Technol., 37, 439-451, doi:10.1016/S0165-232X(03)00083-1, 2003.

Grünewald, T., and Lehning, M.: Altitudinal dependency of snow amounts in two small alpine catchments: can catchment-wide snow amounts be estimated via single snow or precipitation stations? Ann. Glaciol., 52, 153-158, doi:10.3189/172756411797252248, 2011.

Gubler, S., Fiddes, J., Keller, M., and Gruber, S.: Scale-dependent measurement and analysis of ground surface temperature variability in alpine terrain, Cryosphere, 5, 431-443, doi:10.5194/tc-5-431-2011, 2011.

Gupta, H.V., Beven, K., and Wagener, T.: Model calibration and uncertainty estimation, In: Anderson, M.G. (ed.), Encyclopedia of Hydrological Sciences, John Wiley & Sons, Ltd., 305-343, doi:10.1002/0470848944.hsa138, 2005.

Haberkorn, A., Hoelzle, M., Phillips, M., and Kenner, R.: Snow as driving factor of rock surface temperatures in steep rough rock walls, Cold Reg. Sci. Technol., 118, 64-75, doi:10.1016/j.coldregions.2015.06.013, 2015a.

Haberkorn, A., Phillips, M., Kenner, R., Rhyner, H., Bavay, M., Galos, S.P., and Hoelzle, M.: Thermal Regime of Rock and its Relation to Snow Cover in Steep Alpine Rock Walls: Gemsstock, Central Swiss Alps, Geogr. Ann.: Ser. A, 97, 579-597, doi:10.1111/geoa.12101, 2015b.

Hanson, S., and Hoelzle, M.: The Thermal Regime of the Active Layer at the Murtèl Rock Glacier Based on Data from 2002, Permafr. Periglac. Process., 15, 273-282, doi:10.1002/ppp.499, 2004.

Harris, C., Arenson, L.U., Christiansen, H.H., Etzelmüller, B., Frauenfelder, R., Gruber, S., Haeberli, W., Hauck, C., Hölzle, M., Humlum, O., Isaksen, K., Kääb, A., Kern-Lütschg, M.A., Lehning, M., Matsuoka, M., Murton, J.B., Nötzli, J., Phillips, M., Ross, N., Seppälä, M., Springman, S.M., and Vonder Mühll, D.: Permafrost and climate in Europe: Monitoring and modelling thermal, geomorphological and geotechnical responses, Earth-Sci. Rev., 92, 117-171, doi:10.1016/j.earscirev.2008.12.002, 2009.

Hasler, A., Gruber, S., and Haeberli, W.: Temperature variability and offset in steep alpine rock and ice faces, Cryosphere, 5, 977-988, doi:10.5194/tc-5-977-2011, 2011.

Helbig, N., Löwe, H., and Lehning, M.: Radiosity Approach for the Shortwave Surface Radiation Balance in Complex Terrain, J. Atmos. Sci., 66, 2900-2912, doi:10.1175/2009JAS2940.1, 2009.

Hoelzle, M.: Mapping and modelling of mountain permafrost distribution in the Alps, Nor. Geogr. Tidsskr., 50, 11-15, doi:10.1080/00291959608552347, 1996.

Hoelzle, M., Mittaz, C., Etzelmüller, B., and Haeberli, W.: Surface Energy Fluxes and Distribution Models of Permafrost in European Mountain Areas: an Overview of Current Developments, Permafr. Periglac. Process., 12, 53-68, doi:10.1002/ppp.385, 2001.

Imhof, M.: Modelling and Verification of the Permafrost Distribution in the Bernese Alps (Western Switzerland), Permafr. Periglac. Process., 7, 267-280, doi:10.1002/(SICI)1099-1530(199609)7:3<267::AID-PPP221>3.0.CO;2-L, 1996.

Imhof, M., Pierrehumbert, G., Haeberli, W., and Kienholz, H.: Permafrost Investigation in the Schilthorn Massif, Bernese Alps, Switzerland, Permafr. Periglac. Process., 11, 189-206, doi:10.1002/1099-1530(200007/09)11:3<189::AID-PPP348>3.0.CO;2-N, 2000.

Keller, F., and Gubler, H.: Interaction between snow cover and high mountain permafrost, Murtèl-Corvatsch, Swiss Alps, In: Guodong, C. (ed), Proceedings of the 6th International Conference on Permafrost, South China University, Technology Press., 332-337, 1993.

Keller, F., Frauenfelder, R., Gardaz, J.M., Hoelzle, M., Kneisel, C., Lugon, R., Phillips, M., Reynard, E., and Wenker, L.: Permafrost map of Switzerland, In: Lewkowicz, A.G., and Allard, M. (eds), Proceedings of the 7th International Conference on Permafrost, Collection Nordicana, 57, Université Laval, Yellwoknife, Canada, 557-562, 1998.

Kohl, T.: Transient thermal effects below complex topographies, Tectonophys., 306, 311-324, doi:10.1016/S0040-1951(99)00063-3, 1999.

Krautblatter, M., Funk, D., and Günzel, F.K.: Why permafrost rocks become unstable: a rock-ice-mechanical model in time and space, Earth Surf. Process. Landf., 38, 876-887, doi:10.1002/esp.3374, 2013.

Kuonen, P., Bavay, M., and Lehning, M.: Advanced ICTs for Disaster Management and Threat Detection: Collaborative and Distributed Frameworks, chapter POP-C++ and Alpine3D: Petition for a New HPC Approach, IGI Global, doi:10.4018/978-1-61520-987-3.ch015, 2010.

Lehning, M., Bartelt, P., Brown, B., Russi, T., Stöckli, U., and Zimmerli, M.: SNOWPACK model calculations for avalanche warning based upon a new network of weather and snow stations, Cold Reg. Sci. Technol., 30, 145-157, doi:10.1016/S0165-232X(99)00022-1, 1999.

Lehning, M., Bartelt, P., Brown, B., and Fierz, C.: A physical SNOWPACK model for the Swiss avalanche warning Part III: meteorological forcing, thin layer formation and evaluation, Cold Reg. Sci. Technol., 35, 169-184, doi:10.1016/S0165-232X(02)00072-1, 2002a.

Lehning, M., Bartelt, P., Brown, B., Fierz, C., and Satyawali, P.: A physical SNOWPACK model for the Swiss avalanche warning Part II: Snow microstructure, Cold Reg. Sci. Technol., 35, 147-167, doi:10.1016/S0165-232X(02)00073-3, 2002b.

Lehning, M., Völksch, I., Gustafsson, D., Nguyen, T.A., Stähli, M., and Zappa, M.: ALPINE3D: a detailed model of mountain surface processes and its application to snow hydrology, Hydrol. Process., 20, 2011-2128, doi:10.1002/hyp.6204, 2006.

Lehning, M., Löwe, H., Ryser, M., and Raderschall, N.: Inhomogeneous precipitation distribution and snow transport in steep terrain, Water Resour. Res., 44, W07404, doi:10.1029/2007WR006545, 2008.

Luetschg, M., Bartelt, P., Lehning, M., Stoeckli, V. and Haeberli, W.: Numerical simulation of the interaction processes between snow cover and alpine permafrost, In: Phillips, M., Springman, S. and Arenson, L. (eds), Proceedings of the 8th International Conference on Permafrost, Swets & Zeitlinger, Lisse, 697-702, 2003.

Luetschg, M., Lehning, M., and Haeberli, W.: A sensitivity study of factors influencing warm/thin permafrost in the Swiss Alps, J. Glaciol., 54, 696-704, doi:103189/002214308786570881, 2008.

Magnin, F., Deline, P., Ravanel, L., Noetzli, J., and Pogliotti, P.: Thermal characteristics of permafrost in the steep alpine rock walls of the Aiguille du Midi (Mont Blanc Massif, 3842 m a.s.l.), Cryosphere, 9, 109-121, doi:10.5194/tc-9-109-2015, 2015.

Marmy, A., Salzmann, N., Scherler, M., and Hauck, C.: Permafrost model sensitivity to seasonal climatic changes and extreme events in mountainous regions, Environ. Res. Lett., 8, 035048 9pp, doi:10.1088/1748-9326/8/3/035048, 2013.

Maxim Integrated: DS1922L/DS1922T iButton Temperature Loggers with 8KB Data-Log Memory, Maxim Integrated Products, San Jose, 52pp, 2013.

Mittaz, C., Hoelzle, M., and Haeberli, W.: First results and interpretation of energy-flux measurements over Alpine permafrost, Ann. Glaciol., 31, 275-280, doi:10.3189/172756400781820363, 2000.

Mittaz, C., Imhof, M., Hoelzle, M., and Haeberli, W.: Snowmelt Evolution Mapping Using an Energy Balance Approach over an Alpine Terrain, Arct. Antarct. Alp. Res., 34, 274-281, doi:10.2307/1552484, 2002.

Mott, R., and Lehning, M.: Meteorological Modeling of Very High-Resolution Wind Fields and Snow Deposition for Mountains, J. Hydrometeorol., 11, 934-949, doi:10.1175/2010JHM1216.1, 2010.

Mott, R., Egli, L., Grünewald, T., Dawes, N., Manes, C., Bavay, M., and Lehning, M.: Micrometeorological processes driving snow ablation in an Alpine catchment, Cryosphere, 5, 1083-1098, doi:10.5194/tc-5-1083-2011, 2011.

Noetzli, J., and Gruber, S.: Transient thermal effects in Alpine permafrost, Cryosphere, 3, 85-99, doi:10.5194/tc-3-85-2009, 2009.

Noetzli, J., Gruber, S., Kohl, T., Salzmann, N., and Haeberli, W.: Three-dimensional distribution and evolution of permafrost temperatures in idealized high-mountain topography, J. Geophys. Res., 112, F02S13, doi:10.1029/2006JF000545, 2007.

PERMOS: Permafrost in Switzerland 2008/2009 and 2009/2010, Noetzli, J. (ed.), Glaciological Report (Permafrost) No. 10/11 of the Cryospheric Commission of the Swiss Academy of Sciences, pp. 80, 2013.

Phillips, M., Haberkorn, A., Draebing, D., Krautblatter, M., Rhyner, H., and Kenner, R.: Seasonally intermittent water flow through deep fractures in an Alpine Rock Ridge: Gemsstock, Central Swiss Alps, Cold Reg. Sci. Technol., 125, 117-127, doi:10.1016/j.coldregions.2016.02.010, 2016.

Pogliotti, P.: Influence of Snow Cover on MAGST over Complex Morphologies in Mountain Permafrost Regions, Ph.D. thesis, 79 pp., University of Torino, Torino, Italy, 2011.

Ravanel, L., and Deline, P.: Climate influence on rock falls in high-Alpine steep rock walls: The north side of the Aiguilles de Chamonix (Mont Blanc Massif) since the end of the "Little Ice Age", Holocene, 21, 357-365, doi:10.1177/0959683610374887, 2011.

Ravanel, L., Allignol, F., Deline, P., Gruber, S., and Ravello, M.: Rock falls in the Mont Blanc Massif in 2007 and 2008, Recent Landslides, 7, 493-501, doi:10.1007/s10346-010-0206-z, 2010.

Riseborough, D., Shiklomanov, N., Etzelmüller, B., Gruber, S., and Marchenko, S.: Recent Advances in Permafrost Modelling, Permafr. Periglac. Process., 19, 137-156, doi:10.1002/ppp.615, 2008.

Schlögl, S., Marty, C., Bavay, M., and Lehning, M.: Sensitivity of Alpine3D modeled snow cover to modifications in DEM resolution, station coverage and meteorological input quantities, Environ. Modell. Software, xx, xx, doi:10.1016/j.envsoft.2016.02.017, 2016 (accepted).

Schmucki, E., Marty, C., Fierz, C., and Lehning, M.: Evaluation of modelled snow depth and snow water equivalent at three contrasting sites in Switzerland using SNOWPACK simulations driven by different meteorological data input, Cold Reg. Sci. Technol., 99, 27-37, doi:10.1016/j.coldregions.2013.12.004, 2014.

Sommer, C.G., Lehning, M., and Mott, R.: Snow in a very steep rock face: accumulation and redistribution during and after a snowfall event, Front. Earth Sci., 3, Article 73, doi:10.3389/feart.2015.00073, 2015.

Stocker-Mittaz, Hoelzle, M., and Haeberli, W.: Modelling Alpine Permafrost Distribution Based on Energy-Balance Data: a First Step, Permafr. Periglac. Process., 13, 271-282, doi:10.1002/ppp.426, 2002.

Wegmann, M., Gudmundsson, G.H., and Haeberli, W.: Permafrost Changes in Rock Walls and the Retreat of Alpine Glaciers: a Thermal Modelling Approach, Permafr. Periglac. Process., 9, 23-33, doi:10.1002/ppp.615, 1998.

Wever, N., Fierz, C., Mitterer, C., Hirashima, H., and Lehning, M.: Solving Richards Equation for snow improves snowpack meltwater runoff estimations in detailed multi-layer snowpack model, Cryosphere, 8, 257-274, doi:10.5194/tc-8-257-2014, 2014.

Wever, N., Schmid, L., Heilig, A., Eisen, O., Fierz, C., and Lehning, M.: Verification of the multi-layer SNOWPACK model with different water transport schemes, Cryosphere, 9, 2271-2293, doi:10.5194/tc-9-2271-2015, 2015.

Winstral, A., Elder, K., and Davis, R.E.: Spatial Snow Modeling of Wind-Redistributed Snow Using Terrain-Based Parameters, J. Hydrometeorol., 3, 524-538, doi:10.1175/1525-7541(2002)003<0524:SSMOWR>2.0.CO;2, 2002.

Wirz, V., Schirmer, M., Gruber, S., and Lehning, M.: Spatio-temporal measurements and analysis of snow depth in a rock face, Cryosphere, 5, 893-905, doi:10.5194/tc-5-893-2011, 2011.

Zhang, T.: Influence of the seasonal snow cover on the ground thermal regime: An overview, Rev. Geophys., 43, RG4002, doi:10.1029/2004RG0001, 2005.

The Cryosphere Discuss., doi:10.5194/tc-2016-73, 2016
Manuscript under review for journal The Cryosphere
Published: 18 April 2016

Table 1. Topographic characteristics of selected NSRT logger locations with different snow conditions, the distance to the nearest ledge below (DLB), as well as the snow cover duration (Snow).

Location	Elevation (m)	Slope Angle (°)	Aspect (°)	DLB (m)	Snow (months)
N7	2916	90	289	0.1	9
N3	2928	90	284	10	-
S9	2912	72	165	0	9
R2	2934	58	164	15	-

800

The Cryosphere Discuss., doi:10.5194/tc-2016-73, 2016
Manuscript under review for journal The Cryosphere
Published: 18 April 2016

Table 2. Measured and modelled snow cover duration, as well as measured (meas) MANSRT and modelled MANSRT for both snow-covered (mod snow) and snow-free (mod snow-free) conditions at selected NSRT locations and for both years investigated. The MBE were calculated between the measured and modelled snow-covered and the measured and modelled snow-free case.

	Year	Snow cover duration		MANSRT [°C]			MBE [°C]	
		measured	modelled	meas	mod snow	mod snow-free	snow	snow-free
N7	2012-2013	1 Oct-12 Jul	8 Oct-4 Jul	0.1	1.2	-2.5	1.1	-2.6
	2013-2014	6 Oct-12 Jun	9 Oct-14 Jun	0.5	1.7	-1.5	1.2	-1.9
N3	2012-2013	-	-	-1.4	-3.2	-	-1.8	-
	2013-2014	-	-	-0.8	-2.1	-	-1.3	-
S9	2012-2013	27 Oct-7 Jul	28 Oct-14 Jul	2.4	2.3	0.8	-0.1	-1.6
	2013-2014	11 Oct-15 Jun	6 Nov-27 Jun	2.7	2.5	1.8	-0.2	-0.9
R2	2012-2013	-	-	2.8	0.1	-	-2.0	-
	2013-2014	-	-	2.7	1.1	-	-1.6	-

The Cryosphere Discuss., doi:10.5194/tc-2016-73, 2016
Manuscript under review for journal The Cryosphere
Published: 18 April 2016

Table 3. MANSRT, their standard deviation (STD) and MBE [all in °C] calculated within the individual N and S facing rock walls on basis of NSRT locations, as well as on basis of distributed data for the entire slopes (model domain). The MBE was calculated between measured and modelled snow-covered point data and measured and modelled snow-free point data at NSRT locations. MBE for the entire slopes (model domain) was calculated between the modelled snow-covered and modelled snow-free data. Additionally mean annual air temperature (MAAT) for the years 2012-2013 and 2013-2014 is shown.

	1 September 2012-31 August 2013 (2012-2013)			1 September 2013-31 August 2014 (2013-2014)		
Location	MANSRT	STD	MBE	MANSRT	STD	MBE
Measured North	-0.7	1.0		-0.5	0.7	
Modelled North snow	-0.9	1.8	-0.2	-0.4	1.6	0.1
Modelled North snow-free	-2.9	0.7	-2.3	-1.9	0.7	-1.4
Measured South	2.9	0.8		2.7	0.8	
Modelled South snow	1.9	1.2	-0.9	2.1	0.8	-0.7
Modelled South snow-free	0.5	0.9	-1.6	1.3	0.8	-1.2
Modelled N grid snow	-0.7	1.9		-0.3	1.6	-1.5
Modelled N grid snow-free	-2.5	0.8	-2.1	-1.5	0.8	
Modelled S grid snow	2.0	1.1		2.2	1.0	-0.8
Modelled S grid snow-free	0.1	0.9	-1.6	1.1	0.8	
MAAT	-3.2			-2.4		

The Cryosphere Discuss., doi:10.5194/tc-2016-73, 2016
Manuscript under review for journal The Cryosphere
Published: 18 April 2016

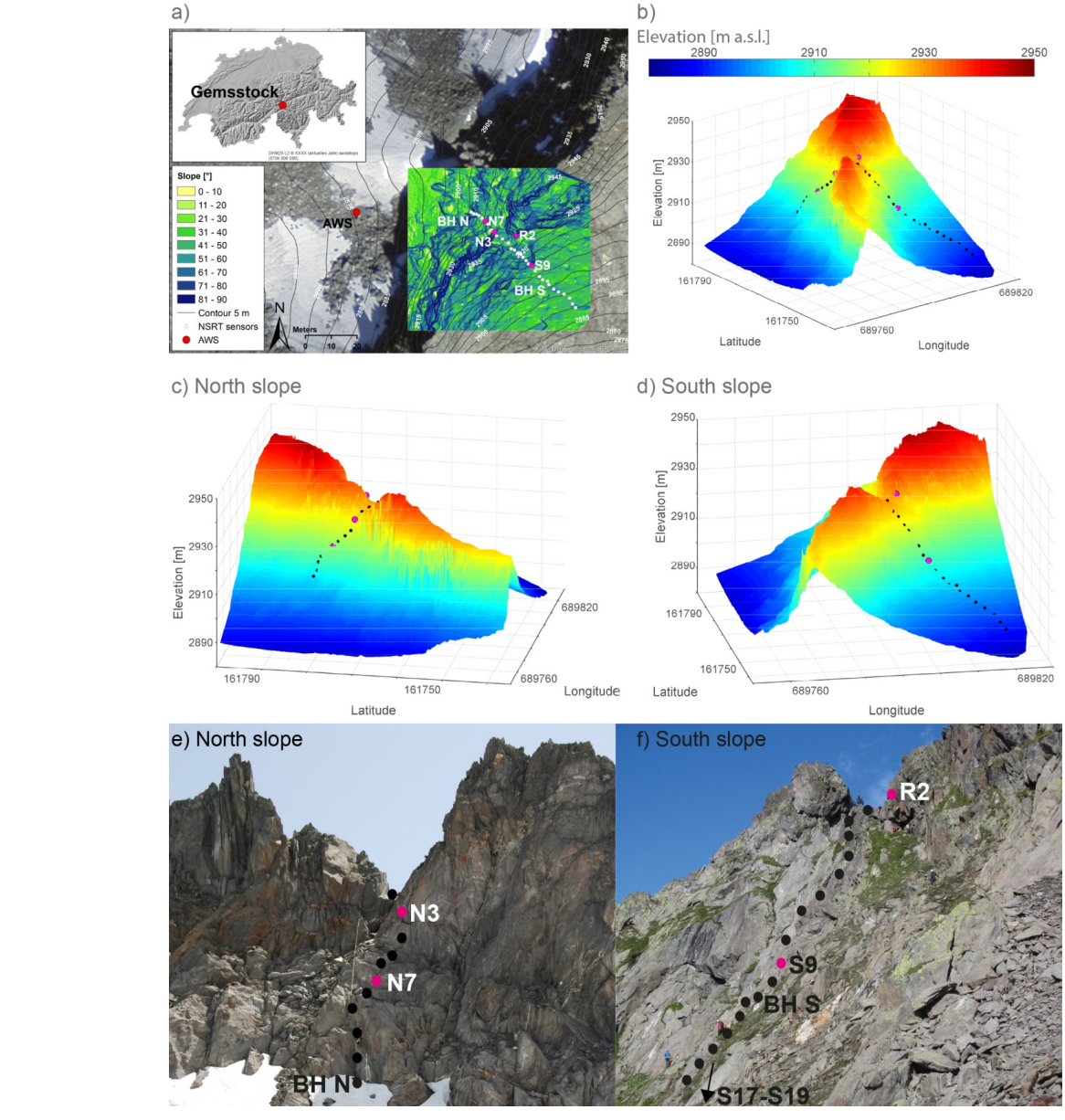

Figure 1. The Gemsstock study area: (a) The extent of the Alpine3D model domain with slope angles based on TLS data, as well as the locations of the AWS, the NSRT devices and borehole ends (BH N and BH S). The location of Gemsstock in the Swiss Alps is shown in the top left inset. 3d profiles based on the DEM of (b) Gemsstock, (c) the N facing- and (d) the S facing rock wall. Photographs, showing the (e) N and (f) S rock faces and the measurement set-up. (b-f) Black dots indicate the locations of the 30 NSRT locations and selected ones, discussed in further detail are highlighted in pink.

The Cryosphere Discuss., doi:10.5194/tc-2016-73, 2016
Manuscript under review for journal The Cryosphere
Published: 18 April 2016

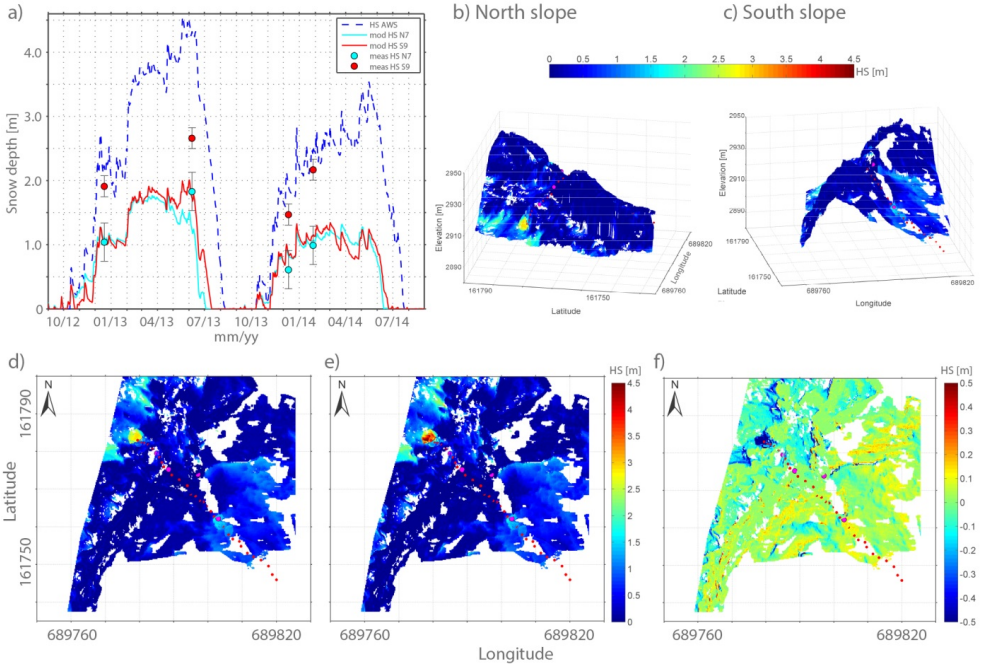

Figure 2. (a) Snow depth evolution measured at the AWS Gemsstock (HS AWS), as well as modelled (mod HS) at the NSRT locations N7 and S9. Snow depths at the NSRT locations obtained by TLS (meas HS) are shown as red and blue dots with error bars. Since the points N3 and R2 are snow-free for the entire investigation period they are not shown. Snow depths (HS) and their distribution on 11 December 2013: 3d TLS data for (b) the N facing and (c) the S facing slopes, as well as 2d data for both the N and the S facing slopes (d) based on TLS, (e) modelled with Alpine3D and (f) their differences (measured - modelled). For better visualization differences are only illustrated here in the range of ±0.5 m, although variations are up to -1 m (only few grid cells). (b-f) Red dots indicate the locations of NSRT loggers and selected ones are highlighted in pink.

The Cryosphere Discuss., doi:10.5194/tc-2016-73, 2016
Manuscript under review for journal The Cryosphere
Published: 18 April 2016

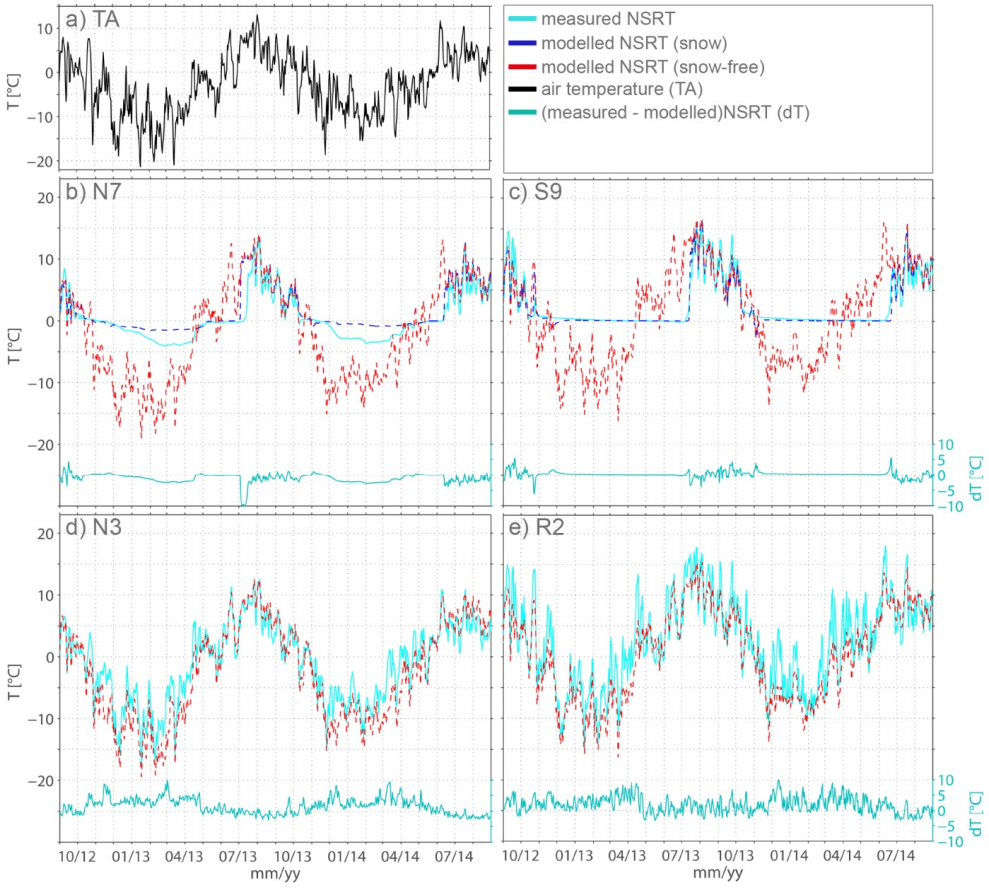

Figure 3. Daily mean air temperature at the AWS Gemsstock (a) and measured and modelled NSRT for snow-covered and snow-free conditions for selected locations in the N and the S facing rock walls (b-e). The differences between measured and modelled NSRT (dT) were calculated for snow-covered conditions in (b) and (c).

The Cryosphere Discuss., doi:10.5194/tc-2016-73, 2016
Manuscript under review for journal The Cryosphere
Published: 18 April 2016

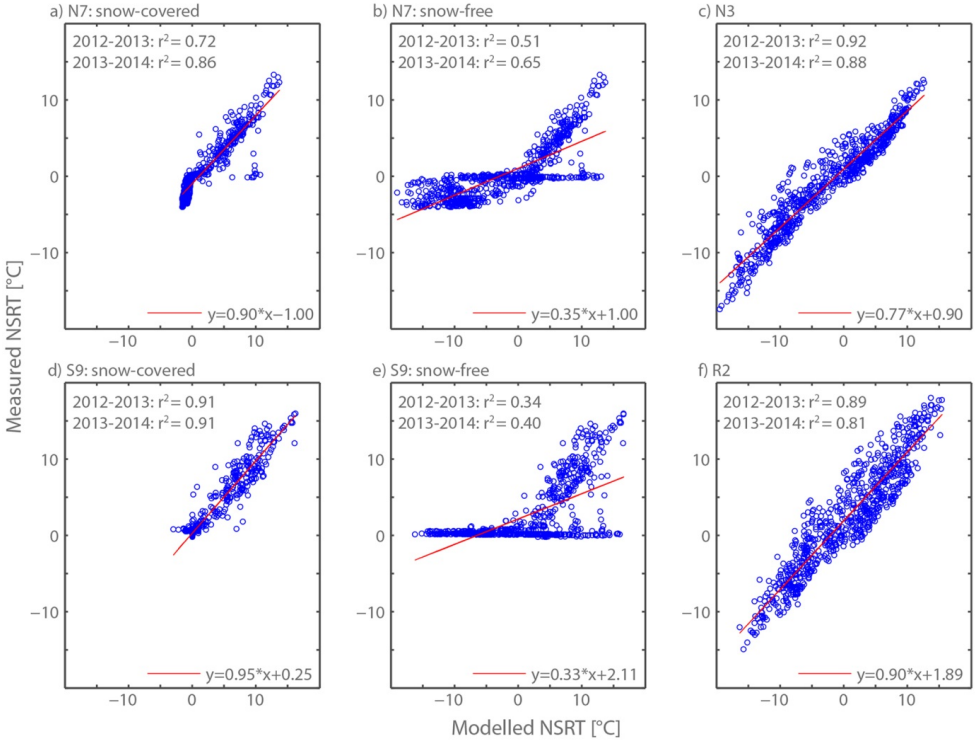

Figure 4. Two year data showing the relation between measured and modelled NSRT data for both snow-covered (a, d) and forced snow-free conditions (b, e), as well as for generally snow-free NSRT locations (c, f). The mean annual r^2, as well as the linear relation between measured and modelled NSRT data are shown.

The Cryosphere Discuss., doi:10.5194/tc-2016-73, 2016
Manuscript under review for journal The Cryosphere
Published: 18 April 2016

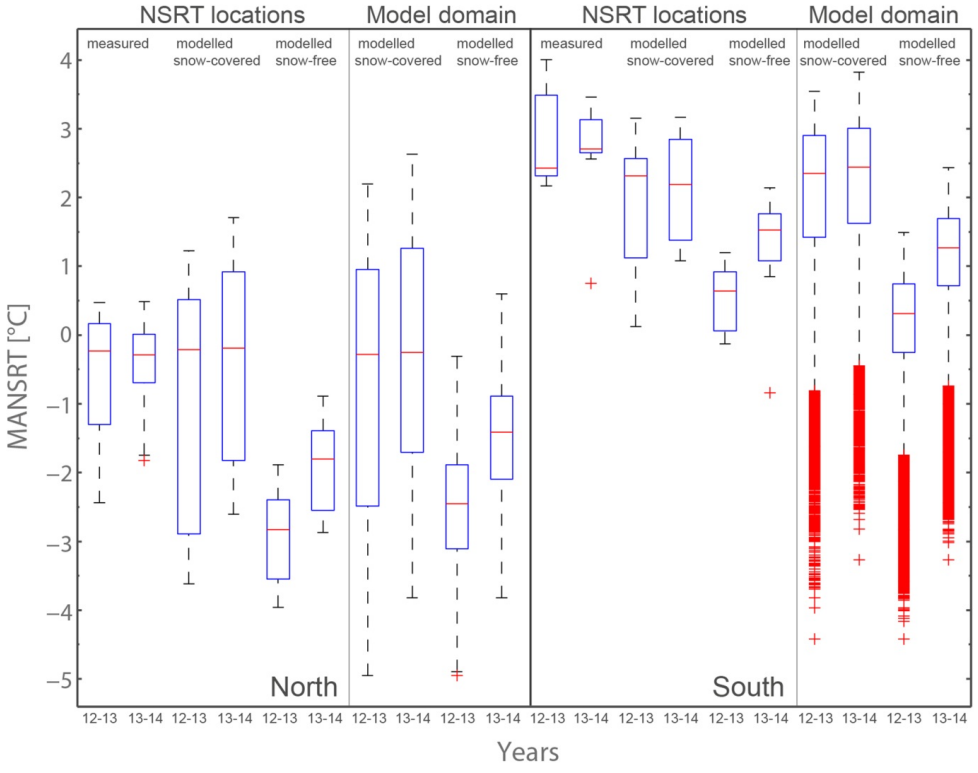

Figure 5. MANSRT variability within the individual N and S facing rock walls calculated at NSRT locations on basis of measured NSRT, as well as modelled NSRT data for both snow-covered and snow-free conditions for the years 2012-2013 (12-13) and 2013-2014 (13-14), as well as modelled MANSRT variability within the entire N and S facing model domain. The median is marked in each box, the box edges are the 25th and the 75th percentiles, the whiskers extend to the 2.5 % and 97.5 % quantiles and outliers are plotted as individual crosses.

The Cryosphere Discuss., doi:10.5194/tc-2016-73, 2016
Manuscript under review for journal The Cryosphere
Published: 18 April 2016

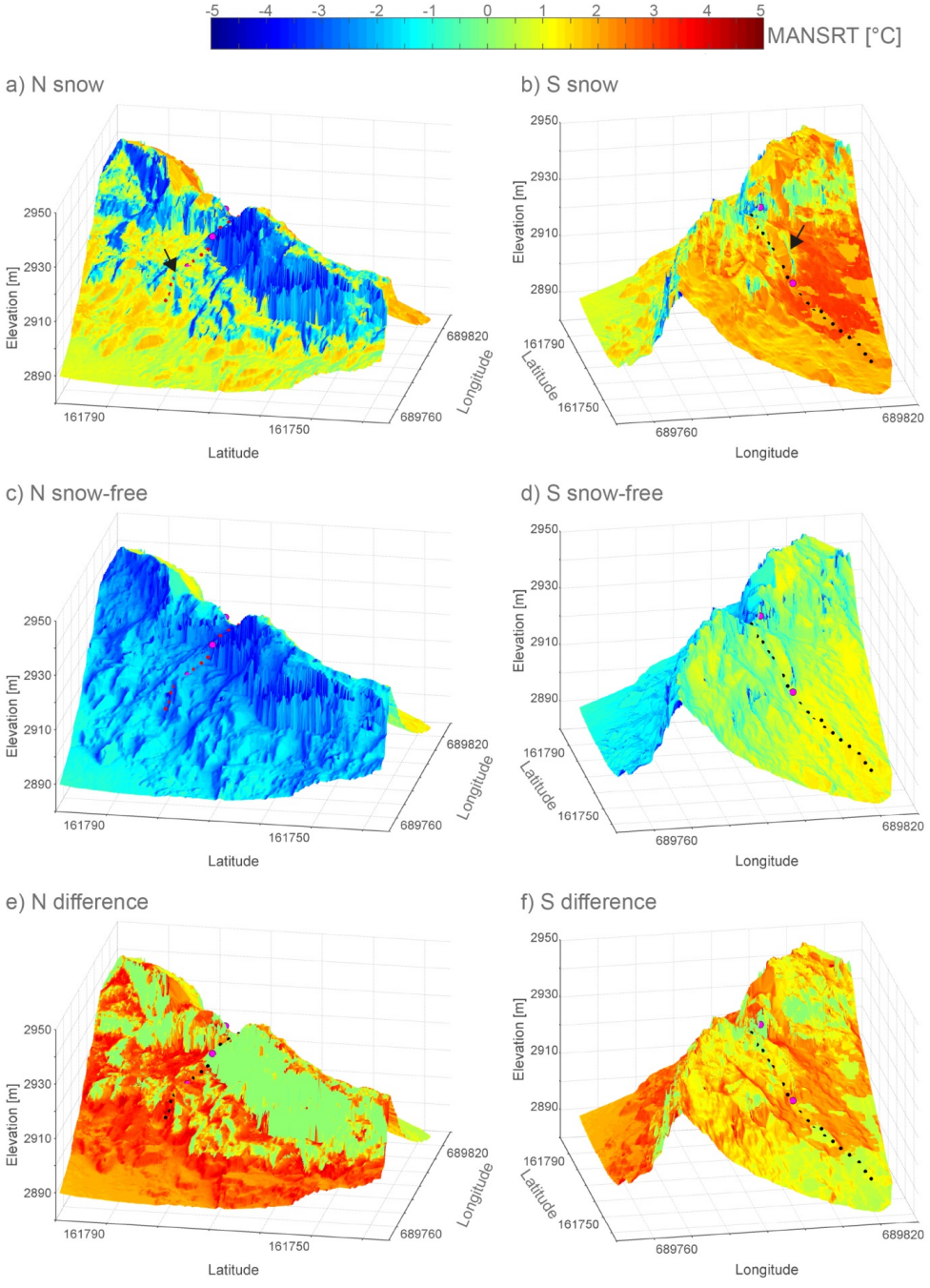

Figure 6. Modelled MANSRT distribution in the N (left) and the S (right) facing slopes for snow-covered conditions (top) and snow-free conditions (middle), as well as their differences (bottom; snow-covered – snow-free). Arrows indicate rock outcrops and rock dihedrals partly shadowing the NSRT locations,

The Cryosphere Discuss., doi:10.5194/tc-2016-73, 2016
Manuscript under review for journal The Cryosphere
Published: 18 April 2016

which are marked by black dots (selected locations in pink). The data is only shown for the year 2012-2013.

The Cryosphere Discuss., doi:10.5194/tc-2016-73, 2016
Manuscript under review for journal The Cryosphere
Published: 18 April 2016

865 **Figure 7. Modelled monthly means of all components of the energy balance for the N facing NSRT location N7 (top) and for the S facing NSRT location S9 (bottom) for snow-covered conditions (left) and snow-free conditions (right).**